The mechanism of size-based particle separation by dielectrophoresis in the viscoelastic flows

Teng Zhou[1a)], Yongbo Deng[2], Hongwei Zhao[3], Xianman Zhang[1], Liuyong Shi[1], Sang Woo Joo[4 a)]

[1]*Mechanical and Electrical Engineering College, Hainan University, Haikou, Hainan Province570228, People's Republic of China*

[2]*Changchun Institute of Optics, Fine Mechanics and Physics (CIOMP), Chinese Academy of Sciences, Changchun, Jilin 130033, People's Republic of China*

[3]*Department of Environmental Science, Hainan University, Haikou, Hainan Province570228, People's Republic of China*

[4] *School of Mechanical Engineering, Yeungnam University, Gyongsan 712-719, Republic of Korea*

Viscoelastic solution is encountered extensively in microfluidics. In this work, the particle movement of the viscoelastic flow in the contraction-expansion channel is demonstrated. The fluid is described by the Oldroyd-B model, and the particle is driven by dielectrophoretic (DEP) forces induced by the applied electric field. A time dependent multiphysics numerical model with the thin electric double layer (EDL) assumption was developed, in which the Oldroyd-B viscoelastic fluid flow field, the electric field and the movement of finite-size particles are solved simultaneously by an Arbitrary Lagrangian–Eulerian (ALE) numerical method. By the numerically validated ALE method, the trajectories of particle with different sizes were obtained for the fluid with the Weissenberg number (Wi) of 1 and 0, which can be regarded as the Newtonian fluid. The trajectory in the Oldroyd-B flow with Wi=1 is compared with that in the Newtonian fluid. Also, trajectories for different particles with different particle sizes moving in the flow with Wi=1 are compared, which proves that the contraction-expansion channel can also be used for particle separation in the viscoelastic flow. The above results for this work provide the physical insight into the particle movement in the flow of viscous and elastic features.

Key Words: Microfluidics, Electrokinetic, Fluid–structure interaction, Computational fluid dynamics (CFD), Arbitrary Lagrangian–Eulerian (ALE) method, viscoelastic flow

1. INTRODUCTION

The microfluidics is proved to be a good tool for sample manipulation in biochemistry field. The particle and cell separation or sorting is one of the pre-requisite steps in the chemical analysis and bioassay [1-8]. In the past decades, many passive [9-12]

[a)] Authors to whom correspondence should be addressed. Electronic addresses: zhouteng@hainu.edu.cn and swjoo@yu.ac.kr

and active microfluidic chips [13-17] were proposed to manipulate particles. Due to its advantages on label-free nature, simplicity of the instrumentation, and analysis of high selectivity and sensitivity [18-21], dielectrophoresis (DEP) phenomenon has been applied to manipulate many different micro/nano-scale bio-entities since the beginning of microfluidics.

Currently, most of the studies for DEP phenomenon are focused on Newtonian fluid. However, many common fluids of interest in the microfluidic field are viscoelastic. The viscoelastic fluid exhibits a mixture of both the viscous and the elastic behavior under strain. These cases related to the visco-elasticity are common in the microfluidic field, e.g. proteins, blood, lipids, growth regulators, and a good deal of the other compounds [22-26]. Being different from that case in Newtonian fluid, the heterogeneous distribution for the first normal stress difference will affect the lateral migration of suspended particles happened in the microfluidic channel, when the particle is moving in the viscoelastic fluid. Due to above difference, previously revealed analytical methods for the 2-D or 3-D particle ordering, focusing and separation study may be not suitable for viscoelastic fluid.

Few theoretical studies have been implemented for particle separation in viscoelastic fluid, especially the study about particle separation by DEP device in the viscoelastic

fluid. Usually, the viscoelastic fluid is simplified to be the Newtonian fluid without considering the visco-elasticity[22, 26]. In this work, we use the Oldroyd-B model to describe the viscoelastic fluid. Coupling with Laplace equation, and the strain energy density function equations, the particle trajectories are obtained by Arbitrary Lagrangian–Eulerian (ALE) numerical method [9, 16, 18, 27], which is validated for different Weissenberg numbers (Wi). By comparing those trajectories for the Oldroyd-B fluid with Wi=0 and 1, the difference of trajectories shows that the simulation of the DEP phenomenon in the non-Newtonian fluid can be simplified by the Newtonian fluid in order to save the computation cost. So it is concluded that the method for size-based particles separation by DEP is also suitable for the non-Newtonian fluid.

The rest of this paper is organized as follows. The theory for the particle trajectory numerical simulation in the Oldroyd-B fluid is presented in Section II. Section III presents the validation of the numerical method. Section IV demonstrates the results of this work. Section V concludes the full paper.

2. Mathematical model

In this study, a two-dimensional (2D) converging-diverging microchannel is conducted to study the particle movement in the incompressible viscoelastic fluid domain

Ω_f shown as Figure 1. A potential difference is externally applied from inlet AJ to outlet FE. Here the outlet EF is grounded. Thus the electric field $\mathbf{E}$ is generated to induce the particle Ω_f to perform electrokinetic motion in this channel. The electric double layer (EDL) thicknesses of the charged particle and microchannel are very thin compared with the particle radius and the width of the microchannel. Thus, the thin EDL approximation can be introduced into this model. As a result, the Laplace equation is used to describe the electrical potential ϕ in the domain Ω_f,

$$\nabla^2\phi = 0 \quad \text{in } \Omega_f \tag{1}$$

Once ϕ is obtained, the local electric field E can be obtained by

$$\mathbf{E} = -\nabla\phi \quad \text{in } \Omega_f \tag{2}$$

The viscoelastic fluid is a dilute polymer solution in a Newtonian liquid solvent of viscosity η_s. Here, two physical parameters are used to characterize the polymer: the viscosity η_p and the relaxation time. The Oldroyd-B constitutive relation which describes the polymer stress contribution $\mathbf{T}$ in the viscoelastic fluid is followed:

$$\mathbf{T} + \lambda\left[\frac{\partial \mathbf{T}}{\partial t} + (\mathbf{u}\cdot\nabla)\mathbf{T} - [(\nabla\mathbf{u})\mathbf{T} + \mathbf{T}(\nabla\mathbf{u})^T]\right] = \eta_p(\nabla\mathbf{u} + \nabla\mathbf{u}^{\mathbf{T}}) \quad \text{in } \Omega_f \tag{3}$$

Here, $\mathbf{u}$ is the fluid velocity, $\mathbf{I}$ is the unit tensor, p is the hydrodynamic pressure, $\nabla\mathbf{u}^{\mathbf{T}}$ is the transpose of $\nabla\mathbf{u}$.

The flow field can be described by the following Navies-Stokes and continuity equation,

$$\rho_f \frac{\partial \mathbf{u}}{\partial t} + \rho_f (\mathbf{u}\cdot)\nabla\mathbf{u} = \nabla\cdot\sigma \quad \text{in } \Omega_f \tag{4}$$

And

$$\nabla\cdot\mathbf{u}=0 \quad \text{in } \Omega_f \tag{5}$$

Here, $\sigma = -p\mathbf{I} + \eta_s(\nabla\mathbf{u} + \nabla\mathbf{u}^{\mathbf{T}}) + \mathbf{T}$ and ρ_f are the total stress and the density of fluid, respectively.

In this work, all the previous governing equations are normalized by following scale: the particle radius r_p as the length scale; the zeta potential ζ_p of the particle surface as the potential scale; $U_0 = (\varepsilon_f \zeta_p / \eta)(\zeta_p / r_p)$ as the velocity scale; $\eta U_0 / r_p$ as the pressure scale, here $\eta = \eta_s + \eta_p$ is total viscosity, ε_f is the fluid permittivity.

So the non-dimensional governing equations system is as follow:

$$\nabla^2\phi^* = 0 \quad \text{in } \Omega_f \tag{6}$$

$$\mathrm{Re}\frac{\partial \mathbf{u}^*}{\partial t^*} + \rho_f (\mathbf{u}^*\cdot)\nabla\mathbf{u}^* = \nabla\cdot\left(-p^*\mathbf{I} + \mu_s(\nabla\mathbf{u}^* + \nabla\mathbf{u}^{*\mathbf{T}}) + \mathbf{T}^*\right) \quad \text{in } \Omega_f \tag{7}$$

$$\nabla\cdot\mathbf{u}^*=0 \quad \text{in } \Omega_f \tag{8}$$

$$\mathbf{T}^* + \frac{\partial \mathbf{T}^*}{\partial t^*} + \mathrm{Wi}\left(\mathbf{u}^*\cdot\nabla\right)\mathbf{T}^* - \left[[(\nabla\mathbf{u}^*)\mathbf{T}^* + \mathbf{T}^*(\nabla\mathbf{u}^*)^T]\right] = \mu_p(\nabla\mathbf{u}^* + \nabla\mathbf{u}^{*\mathbf{T}}) \quad \text{in } \Omega_f \tag{9}$$

Here, $\mu_s = \eta_s / \eta$ and $\mu_p = \eta_p / \eta = 1 - \mu_s$ are the relative viscosities of the solvent and polymer. Wi=$\lambda U_0 / r_p$ is the Weissenberg number. A zero Wi corresponds to no elastic response, while Wi> 1 can be considered as a high Wi for many Oldroyd-B fluid.

The corresponding boundary conditions for the above governing equation are following:

$$\phi^* = \phi_0 / \zeta_p \quad \text{on } AJ \tag{10}$$

$$\phi^* = 0 \quad \text{on EF} \tag{11}$$

Assuming that the other solid boundaries which include the channel wall (Γ_w) and particle surface (Γ_p) are electrically insulating, resulting in:

$$\mathbf{n} \cdot \nabla \phi^* = 0 \text{ on } \Gamma_w \text{ and } \Gamma_p \tag{12}$$

Here **n** is the outward normal vector.

The open boundary is set as the inlet and outlet of this system, that is,

$$\sigma^* \cdot \mathbf{n} = 0 \cdot \mathbf{n} \quad \text{on AJ, EF} \tag{13}$$

The slip boundary of the Smoluchowski electroosmotic flow (EOF) velocity is set to be the velocity of the charged channel wall,

$$\mathbf{u}^* = \mathbf{u}^*_w = \frac{\zeta_w}{\zeta_p} (\mathbf{I} - \mathbf{nn}) \cdot \nabla \phi \quad \text{on } \Gamma_w \tag{14}$$

$$\left(\mathbf{T}^* \cdot \mathbf{n}\right) \cdot \mathbf{n} = 0 \tag{15}$$

In the above, u^*_w is the dimensionless fluid velocity on the channel wall.

The particle velocity $\mathbf{u}_p$ is consisted of two parts, which are (a) the Smoluchowski slip velocity caused by the particle's surface charge and (b) the particle movement velocity. Therefore, the boundary condition in fluid field of the particle surface is

$$\mathbf{u}^* = \mathbf{u}^*_p = (\mathbf{I} - \mathbf{nn}) \cdot \nabla \phi^* + \frac{\partial \mathbf{w}^*}{\partial t^*} \quad \text{on } \Gamma_p \tag{16}$$

In the above, ζ_p is the zeta potential of the particle, and is the displacement of the deformable particle arising from the particle movement and deformation, which are can be described by the hyper elastic mechanics.

3. Numerical Method and Validation of Numerical Model

The model presented in this paper is solved by the commercial finite element package COMSOL Multiphysics numerically (www.comsol.com) coupled with MATLAB which is run in a high performance workstation. In order to keep the accuracy of results, all the governing equations inside are solved by coupling method. The value of minimum mesh quality in the domain is the criterion to control the mesh. When the value of mesh quality is below 0.7 (the highest mesh quality of a finite element is 1.0), the domain is re-meshed and the solution is mapped to a new geometry to maintain the regularity of geometry and

mesh. By the above method, the particle with different shear modules can be obtained by steps of iteration.

To validate the present method, we conduct the benchmark problem in the flow of Oldroyd-B fluid past a circular cylinder place between parallel fixed plates to compare the result in the paper published by Behr et al[28]. In the benchmark, the model is non-dimensionalized. The radius of the cylinder is taken as R = 1, and the channel width as h = 16. The fluid and solvent viscosities are $\mu_s = 0.41$ and $\mu_p = 0.59$ respectively. A parabolic flow profile is applied on the inlet with the maximum flow rate is 1.5. The drag force for Weissenberg numbers 0.0 to 2.0 is shown in Figure 2a. It is indicated that the agreement between our model (solid line) and results (symbol) of Behr et al is excellent from Wi of 0 up to 2.

Furthermore, the results are compared with the existing analytical results about the electrophoresis of a rigid spherical particle with the diameter d along the axis of an infinite long tube of diameter a obtained by Keh and Anderson [29]. Neglecting the DEP force, the approximate analytical solution under the conditions of thin EDL for the electrophoretic velocity of a spherical particle (U_p) is

$$U_p = \left[1 - 1.28987\left(\frac{d}{a}\right)^3 + 1.89632\left(\frac{d}{a}\right)^5 - 1.02780\left(\frac{d}{a}\right)^6\right]\left(1 - \frac{\zeta_w}{\zeta_p}\right)U_0 \qquad (17)$$

where $U_0 = \varepsilon_f \zeta_p E_z / \mu$ is the Smoluchowski velocity with the external electric field axial strength E_z in the absence of particles. Here, $E_z = 3$ KV , $\zeta_w = 60$ mV , $\zeta_p = 20$ mV , $\varepsilon_f = 7.08\times10^{-10}$ F/m , $\rho_f = 1000$ kg/m^3 and $\mu = 0.001$ Pa·s in the benchmark. As shown in Fig. 2b, the present numerical results of U_p (symbols) agree well with the analytical solution of Keh and Anderson (solid line). The above two validations imply that the performance of the present model is satisfactory.

4. Result and discussion

Using the above validated numerical method, the parametric study has been conducted to make an insight of particle movement in the Oldroyd-B viscoelastic flow. According to the result we obtained, it is found that the DEP particle separation method work similarly in the viscoelastic flow as the Newtonian flow due to the low Reynolds number in the DEP phenomenon. In this section, the entire length of the symmetric converging-diverging channel is 400μm, with L_a=L_d=125μm and L_b=L_c=75μm. The width of the uniform section and throat are set to w=200μm and b=50μm. The initial transverse location of the particle is d_p=10μm. Furthermore, the radius of the largest particle in the work is r_{pmax}=5μm, used as the length scale. So after being normalized, the parameter for the geometry is following: L_a^*=L_d^*=25, L_b^*=L_c^*=15, w^*=40, b^*=10, d_p^*=2.

We calculate the applied electric field strength E which can be obtained by dividing the inlet and outlet electric potential difference over the microchannel total length. In this study, the E is set to 10KV/m. The physical properties of the solution used in the simulation are $\rho_f = 1000$ kg/m^3, $\mu = 0.001$ Pa·s and $\varepsilon_f = 7.08\times10^{-10}$ F/m. We assume that the density and the permittivity of the deformable particle are the same as the solution, which means that $\rho_p = 1000$ kg/m^3 and $\varepsilon_p = 7.08\times10^{-10}$ F/m. The zeta potentials of the channel wall (ζ_w) is assumed to be -80 mV, and the zeta potentials of the particle (ζ_p) is -15 mV respectively, used as the potential scale. Besides, the non-dimensional fluid and solvent viscosities are $\mu_s = 0.59$ and $\mu_p = 0.41$, respectively.

4.1 Trajectory differences between Newtonian flow and Non-Newtonian flow

Particle trajectories for different radius in the Non-Newtonian flow with Wi=0 and 1 are studied by the validated ALE method mentioned before. The series of particle radius is 5μm, 4μm, 3μm and 2μm. The radius r_p=5μm is chosen as the length scale. So the non-dimensional normalized particle radiuses r_p^* are 1, 0.8, 0.6, and 0.4. The ratio of the width to the particle radius w^* / r_p^* is 40, 50, 66.7 and 100, respectively. The particle trajectories for each particle radius are shown as Fig.3 (a)-(d).

In the simulation, the Weissenberg number is set to 0 and 1, while the fluid with a zero Wi corresponds to Newtonian flow. Form the result of Fig.3, it is shown that

particles migrate to the center, both in Newtonian flow and Non-Newtonian flow. It means that the DEP phenomenon still exists in the Non-Newtonian flow. In the study before, it is reported that the reason that the particle migrates to the center after passing the throat is mainly the DEP force. Whether in the Newtonian flow or Non-Newtonian flow, the DEP force is generated by the applied electric field and can be calculated by integration of the Maxwell tensor. Therefore, the DEP forces on the particle are almost equal in Newtonian flow and Non-Newtonian flow if other identical settings are employed. However, the particle movement is driven by both the DEP force and the hydrodynamic force. When the particle moves in the channel, the fluid field is not only time dependent but also space dependent. Because of the elasticity of the Oldroyd-B flow, the non-dimensional hydrodynamic force on the particle in viscoelastic flow is slightly different from that in the Newtonian flow, as shown in Fig 4. Thus the particle trajectory shift is slightly different when the particle goes through the throat between the Non-Newtonian flow and the viscoelastic flow. However, the difference of particle trajectories can even be neglected compared to channel width. While the value of w^* / r_p^* changes from 40 to 100, the difference of y coordinate for the trajectories after going through the throat is only 0.60, 0.49, 0.17 and 0.82, respectively. So that even though the difference changes with the value of w^* / r_p^*, it is less than one particle radius. As a result, in order

to make the computing cost lower and the design more easily, we can use the Newtonian flow setting instead of the viscoelastic flow setting in this DEP phenomenon which dominates the particle movement in the channel.

4.2 Force differences between Newtonian flow and Non-Newtonian flow

The difference of particle trajectories is caused by the force difference on the particle surface. In the fluid field, the stress tensor on the particle surface is comprised of two parts: the fluid reaction stress tensor and the Maxwell stress tensor. As mentioned above, the Maxwell stress on the particle surface is equal if other settings are identical, for example, shape and size of particle, fluid domain, the applied electric field and so on. Thus, the difference of particle trajectories is accurately caused by the hydrodynamic force on the particle in the channel.

In order to depict that the hydrodynamic force on the particles changes with the Weissenberg numbers, we calculate the hydrodynamic force in the *x* and *y* direction fluid with two different Wi: 0 and 1. The particle position is picked up from the trajectory for Wi=1 in Fig. 3a. In order to compare the force with different Wi, the particles are supposed as stationery without including the movements. So the boundary condition for the flow on the particles surface is non-slip condition, and others setting are identical as the above simulation for the case with $r_p^* = 1$. The hydrodynamic force of the particle

surface is obtained by integration of hydrodynamic stress tensor on the interaction boundary; then the value of force is normalized by the maximum of absolute value of each component. Figure 4a shows the *x* component of force in the main flow direction for the case of Wi=0 and 1. The *x* component of force for Wi=0 is a little larger than that of Wi=0. Moreover, the difference occurs after the throat of the channel. It means that the particle will move with approximate velocity before and in the throat in the main flow direction. And also, *y* component of the hydrodynamic force in the lateral migration direction of the case with Wi=1 is a bit larger than that of the case with Wi=0, especially near the throat, as shown from the Fig. 4b. The result means that the particle will be pushed farther away from the wall in the Newtonian flow than in the viscoelastic flow. However, the difference of the force is not obvious. Thus the difference of the particle trajectories just plays a bit of role resulting in the trajectories migration shift in the Fig. 3.

4.3 Effect of particle size

The trajectories for the particles with different sizes are shown in Fig. 5, where the particles move from inlet to outlet driven by DEP force in the viscoelastic flow. As discussed above, it is the DEP force that pushes the particle move across the streamline, which varies with the cubic of the particle size. Because that the DEP force diminishes with the decreasing of particle sizes, the lateral migration of particle also decrease with

the reducing of the particle radius. As the above phenomenon, the trajectories of particles with different radius are different in the viscoelastic flow (Fig. 5), that means the converging-diverging microchannel still have the application potential for being used for particle separation in the viscoelastic flow.

5. Conclusions

The particle electrophoretic motion due to the effect of DEP force caused by the non-uniform electric field through a contraction-expanding channel microchannel in the viscoelastic flow is numerically investigated using a time dependent ALE finite element numerical model. The Oldroyd-B model is used to describe the viscoelastic fluid. And the particle trajectories along the converging–diverging microchannel in the viscoelastic fluid flow with different Weissenberg numbers are obtained by the validated ALE method. Furthermore, the hydrodynamic force for different Weissenberg numbers is also obtained. The result shows that the effect of elasticity for the viscoelastic flow can be neglected in the DEP phenomenon, comparing with the Newtonian fluid. Particles at first is far from the center of the microchannel and then move toward the centerline of the channel in the downstream, which means that the converging–diverging microchannel still can be applied on particle focusing in the viscoelastic flow. Because the particles with different

sizes own different trajectories, the converging–diverging microchannel has large potential for the continuous manipulation of biological particle e.g. DNAs and cells, for both Newtonian fluid and viscoelastic fluid.

Acknowledgements

This work was partially supported by National Natural Science Foundation of China (Grant No. 51605124), National Research Foundation of Korea (Grant No.2015-002423) and the Scientific Research Foundation of Hainan University (Grant No.Kyqd1569, hdkyxj201721 and hdkyxj201722)

References

[1] Ai, Y., and Qian, S., 2010, "DC dielectrophoretic particle-particle interactions and their relative motions.," Journal of colloid and interface science, 346, pp. 448-454.
[2] Ai, Y., Mauroy, B., Sharma, A., and Qian, S., 2011, "Electrokinetic motion of a deformable particle: dielectrophoretic effect.," Electrophoresis, 32, pp. 2282-2291.
[3] Xuan, X., Zhu, J., and Church, C., 2010, "Particle focusing in microfluidic devices," Microfluidics and Nanofluidics, 9(1), pp. 1-16.
[4] Martel, J. M., and Toner, M., 2014, "Inertial focusing in microfluidics," Annual Review of Biomedical Engineering, 16(1), pp. 371-396.
[5] Tripathi, S., Kumar, Y. V. B. V., Prabhakar, A., Joshi, S. S., and Agrawal, A., 2015, "Passive blood plasma separation at the microscale: a review of design principles and microdevices," Journal of Micromechanics and Microengineering, 25(8), p. 083001.
[6] Ostad, M. A., Hajinia, A., and Heidari, T., 2017, "A novel direct and cost effective method for fabricating paper-based microfluidic device by commercial eye pencil and its application for determining simultaneous calcium and magnesium," Microchemical Journal, 133, pp. 545-550.

[7] Fernández-Baldo, M. A., Ortega, F. G., Pereira, S. V., Bertolino, F. A., Serrano, M. J., Lorente, J. A., Raba, J., and Messina, G. A., 2016, "Nanostructured platform integrated into a microfluidic immunosensor coupled to laser-induced fluorescence for the epithelial cancer biomarker determination," Microchemical Journal, 128, pp. 18-25.
[8] de Oliveira Magalhães, L., and Fonseca, A., 2017, "A microfluidic device with ion-exchange preconcentration column and photometric detection with Schlieren effect correction," Microchemical Journal, 132, pp. 161-166.
[9] Zhou, T., Liu, Z., Wu, Y., Deng, Y., Liu, Y., and Liu, G., 2013, "Hydrodynamic particle focusing design using fluid-particle interaction," Biomicrofluidics, 7, p. 054104.
[10] Zhou, T., Xu, Y., Liu, Z., and Joo, S. W., 2015, "An enhanced one-layer passive microfluidic mixer with an optimized lateral structure with the Dean effect," Journal of Fluids Engineering, 137(9), p. 091102.
[11] Zhang, J., Yan, S., Yuan, D., Alici, G., Nguyen, N.-T., Warkiani, M. E., and Li, W., 2016, "Fundamentals and applications of inertial microfluidics: a review," Lab on a Chip, 16(1), pp. 10-34.
[12] Zhang, Z., Henry, E., Gompper, G., and Fedosov, D. A., 2015, "Behavior of rigid and deformable particles in deterministic lateral displacement devices with different post shapes," Journal of Chemical Physics, 143(24), pp. 243145-243145.
[13] Hallfors, N. G., Alhammadi, F., and Alazzam, A., "Deformation of red blood cells under Dielectrophoresis," Proc. Bio-engineering for Smart Technologies (BioSMART), 2016 International Conference on, IEEE, pp. 1-3.
[14] Sajeesh, P., and Sen, A. K., 2013, "Particle separation and sorting in microfluidic devices: a review," Microfluidics and Nanofluidics, 17(1), pp. 1-52.
[15] Zhang, C., Khoshmanesh, K., Mitchell, A., and Kalantarzadeh, K., 2009, "Dielectrophoresis for manipulation of micro/nano particles in microfluidic systems," Analytical and Bioanalytical Chemistry, 396(1), pp. 401-420.
[16] Zhou, T., Yeh, L.-H., Li, F.-C., Mauroy, B., and Joo, S., 2016, "Deformability-Based Electrokinetic Particle Separation," Micromachines, 7(9), p. 170.
[17] Zhou, T., Liu, T., Deng, Y., Chen, L., Qian, S., and Liu, Z., 2017, "Design of microfluidic channel networks with specified output flow rates using the CFD-based optimization method," Microfluidics and Nanofluidics, 21(1), p. 11.
[18] Zhou, T., Shi, L., Fan, C., Liang, D., Weng, S., and Joo, S. W., 2017, "A novel scalable microfluidic load sensor based on electrokinetic phenomena," Microfluidics and Nanofluidics, 21(4), p. 59.

[19] Zhou, T., Wang, H., Shi, L., Liu, Z., and Joo, S., 2016, "An Enhanced Electroosmotic Micromixer with an Efficient Asymmetric Lateral Structure," Micromachines, 7(12), p. 218.
[20] Ai, Y., Qian, S., Liu, S., and Joo, S. W., 2010, "Dielectrophoretic choking phenomenon in a converging-diverging microchannel.," Biomicrofluidics, 4, p. 13201.
[21] Dubose, J., Lu, X., Patel, S., Qian, S., Woo Joo, S., and Xuan, X., 2014, "Microfluidic electrical sorting of particles based on shape in a spiral microchannel.," Biomicrofluidics, 8, p. 014101.
[22] Zhao, C., and Yang, C., 2013, "Electrokinetics of non-Newtonian fluids: A review," Advances in Colloid and Interface Science, 201–202, pp. 94-108.
[23] Lu, X., Joo, S.-W., Qian, S., and Xuan, X., 2013, "Electrokinetic particle motions in non-Newtonian fluids through a microchannel contraction," Bulletin of the American Physical Society, 58.
[24] Villone, M. M., Greco, F., Hulsen, M. A., and Maffettone, P. L., 2016, "Numerical simulations of deformable particle lateral migration in tube flow of Newtonian and viscoelastic media," Journal of Non-newtonian Fluid Mechanics, 234, pp. 105-113.
[25] Li, X.-B., Oishi, M., Matsuo, T., Oshima, M., and Li, F.-C., 2016, "Measurement of Viscoelastic Fluid Flow in the Curved Microchannel Using Digital Holographic Microscope and Polarized Camera," Journal of Fluids Engineering, 138(9), p. 091401.
[26] D'Avino, G., Greco, F., and Maffettone, P. L., 2017, "Particle Migration due to Viscoelasticity of the Suspending Liquid and Its Relevance in Microfluidic Devices," Annual Review of Fluid Mechanics, 49(1), pp. 341-360.
[27] Zhou, T., Ge, J., Shi, L., Fan, J., Liu, Z., and Woo Joo, S., 2018, "Dielectrophoretic choking phenomenon of a deformable particle in a converging-diverging microchannel," ELECTROPHORESIS, 39(4), pp. 590-596.
[28] Behr, M., Arora, D., Coronado, O., and Pasquali, M., "GLS-type finite element methods for viscoelastic fluid flow simulation," Proc. Proc of the Third MIT Conference on Computational Fluid and Solid Mechanics, Massachusetts Institute of Technology, Cambridge, USA, pp. 135-308.
[29] Keh, H., and Anderson, J., 1985, "Boundary effects on electrophoretic motion of colloidal spheres," Journal of Fluid Mechanics, 153, pp. 417-439.

Journal of Fluids Engineering. Received October 11, 2017;
Accepted manuscript posted March 22, 2018. doi:10.1115/1.4039709

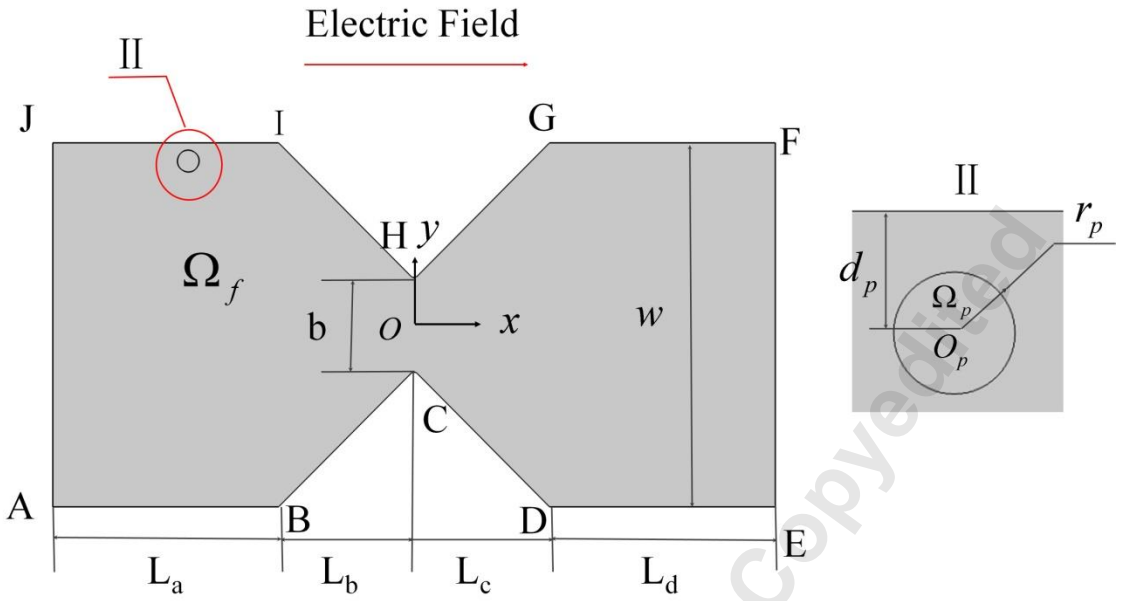

Figure 1.Sketch of the electrokinetic motion for a spherical particle of radius r_p and zeta potential ζ_p in a converging–diverging microchannel with zeta potential ζ_w. Here, *w* is the width of the main channel, and the widths of channel with outlet/inlet AJ and FE are same; b is the width of the throat; d_p is the distance between the nearest channel wall and the center of the spherical particle.

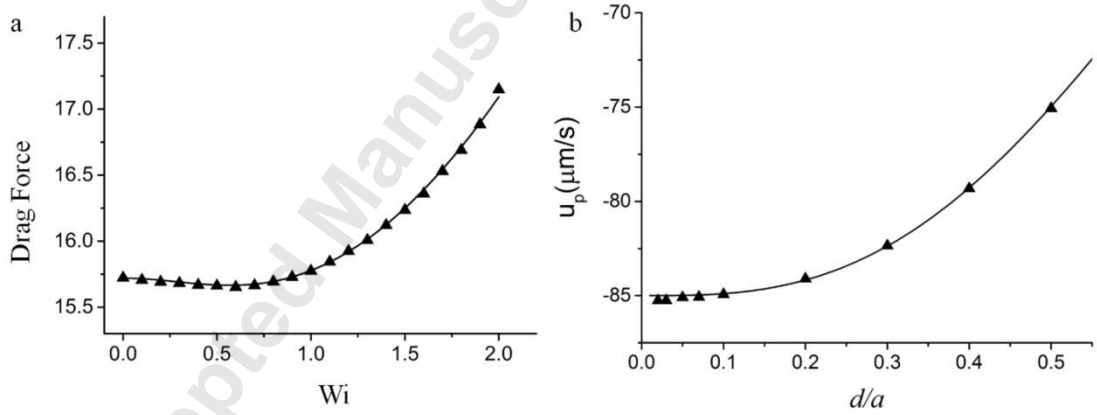

Figure 2.(a) The drag force as the function of the Weissenberg number for the flow past a circular cylinder. The triangle symbols and solid line represent the simulation solution of Behr et al [28] and the numerical results from the present model, respectively (b) Velocity of a sphere particle moving along the cylindrical tube axis as a function of the ratio between the sphere diameter d and the channel diameter a. The solid line and triangle symbols respectively represent the analytical solution of Keh and Anderson [29] and our present model numerical results.

Journal of Fluids Engineering. Received October 11, 2017;
Accepted manuscript posted March 22, 2018. doi:10.1115/1.4039709

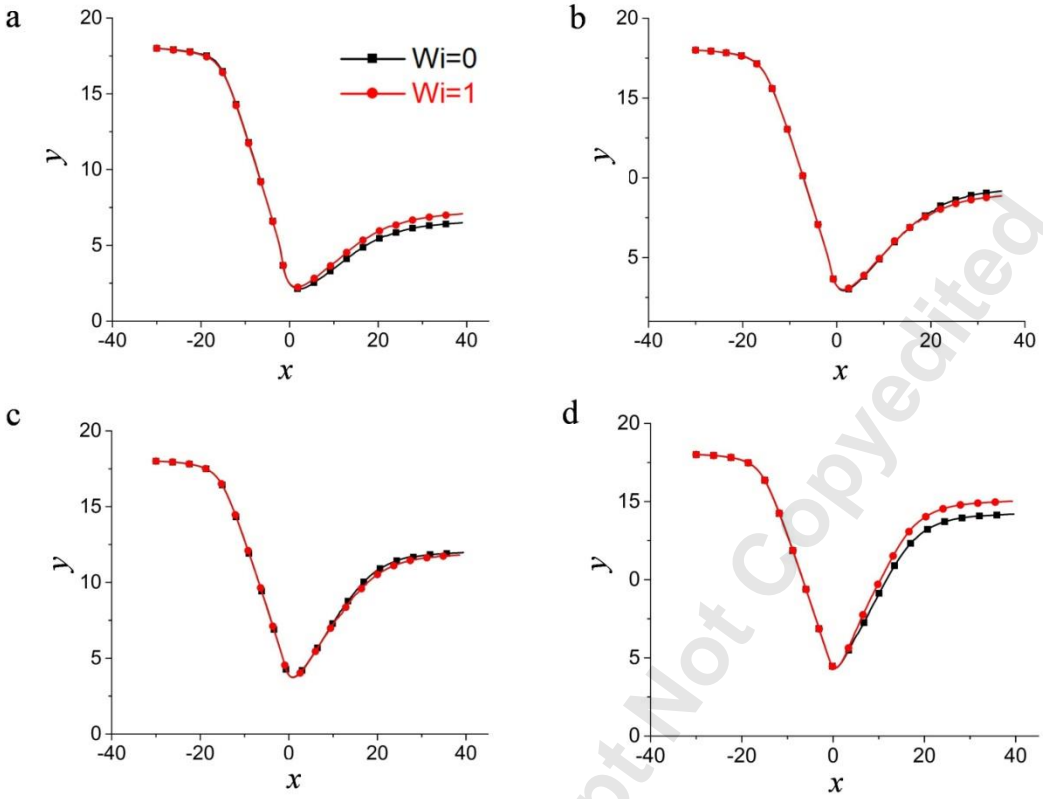

Figure 3 Particle trajectories in the Non-Newtonian flow with Wi=0 and 1, while the Non-Newtonian flow with Wi=0 can be regarded as Newtonian flow. The non-dimensional radiuses of particle are following: (a) $r_p^* = 1$ (b) $r_p^* = 0.8$ (c) $r_p^* = 0.6$ (d) $r_p^* = 0.4$, the length of axis for each sub figure is identical.

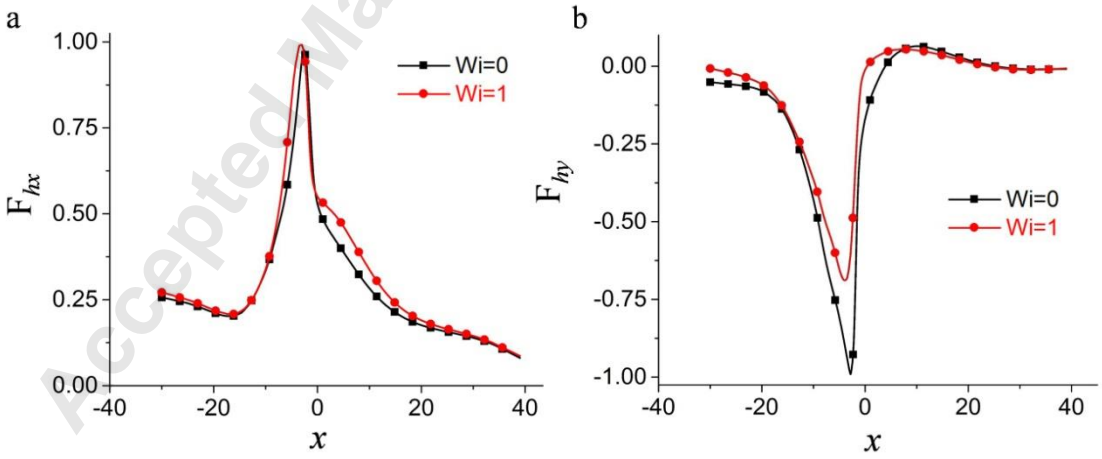

Figure 4 The hydrodynamic force of particle surface calculated by integration of hydrodynamic stress tensor of the interaction face, which have been normalized by the maximum of absolute value of each component (a) x component, in the main flow direction (b) y component, in the lateral migration direction.

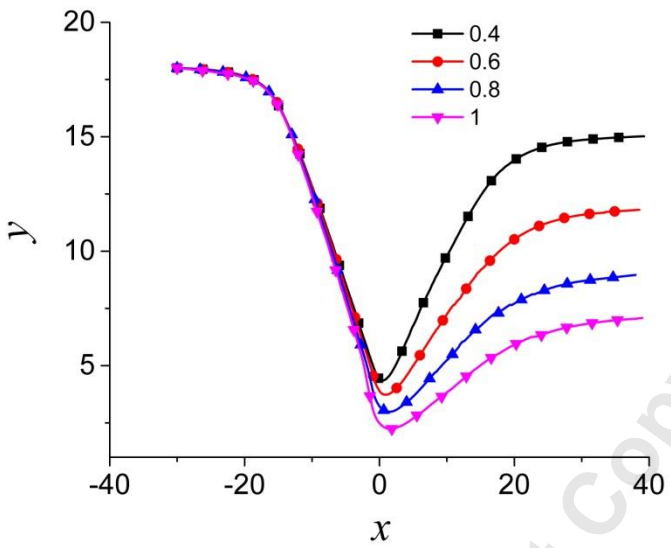

Figure 5 Particle trajectories in the Non-Newtonian flow with Wi= 1. The non-dimensional radiuses of particle r_p^* for each trajectory are 0.4, 0.6, 0.8, and 1, respectively.

Figure list:

Figure 1.Sketch of the electrokinetic motion for a spherical particle of radius r_p and zeta potential ζ_p in a converging–diverging microchannel with zeta potential ζ_w. Here, *w* is the width of the main channel, and the widths of channel with outlet/inlet AJ and FE are same; b is the width of the throat; d_p is the distance between the nearest channel wall and the center of the spherical particle.

Figure 2.(a) The drag force as the function of the Weissenberg number for the flow past a circular cylinder. The triangle symbols and solid line represent the simulation solution of Behr et al [28] and the numerical results from the present model, respectively (b) Velocity of a sphere particle moving along the cylindrical tube axis as a function of the ratio between the sphere diameter d and the channel diameter a. The solid line and triangle symbols respectively represent the analytical solution of Keh and Anderson [29] and our present model numerical results.

Figure 3 Particle trajectories in the Non-Newtonian flow with Wi=0 and 1, while the Non-Newtonian flow with Wi=0 can be regarded as Newtonian flow. The non-dimensional radiuses of particle are following: (a) $r_p^* = 1$ (b) $r_p^* = 0.8$ (c) $r_p^* = 0.6$ (d) $r_p^* = 0.4$, the length of axis for each sub figure is identical.

Figure 4 The hydrodynamic force of particle surface calculated by integration of hydrodynamic stress tensor of the interaction face, which have been normalized by the maximum of absolute value of each component (a) x component, in the main flow direction (b) y component, in the lateral migration direction.

Figure 5 Particle trajectories in the Non-Newtonian flow with Wi= 1. The non-dimensional radiuses of particle r_p^* for each trajectory are 0.4, 0.6, 0.8, and 1, respectively.